Tropical Cyclones in Rotating Radiative–Convective Equilibrium with Coupled SST

WENYU ZHOU[a]

Atmospheric and Oceanic Sciences Program, Princeton University, Princeton, New Jersey

ISAAC M. HELD AND STEPHEN T. GARNER

NOAA/Geophysical Fluid Dynamics Laboratory, Princeton, New Jersey

(Manuscript received 1 July 2016, in final form 19 December 2016)

ABSTRACT

Tropical cyclones are studied under the idealized framework of rotating radiative–convective equilibrium, achieved in a large doubly periodic *f* plane by coupling the column physics of a global atmospheric model to rotating hydrostatic dynamics. Unlike previous studies that prescribe uniform sea surface temperature (SST) over the domain, SSTs are now predicted by coupling the atmosphere to a simple slab ocean model. With coupling, SSTs under the eyewall region of tropical cyclones (TCs) become cooler than the environment. However, the domain still fills up with multiple long-lived TCs in all cases examined, including at the limit of the very small depth of the slab. The cooling of SSTs under the eyewall increases as the depth of the slab ocean layer decreases but levels off at roughly 6.5 K as the depth approaches zero. At the eyewall, the storm interior is decoupled from the cooler surface and moist entropy is no longer well mixed along the angular momentum surface in the boundary layer. TC intensity is reduced from the potential intensity computed without the cooling, but the intensity reduction is smaller than that estimated by a potential intensity taking into account the cooling and assuming that moist entropy is well mixed along angular momentum surfaces within the atmospheric boundary layer.

1. Introduction

Radiative–convective equilibrium (RCE) is a useful idealized framework for studying the tropical atmosphere. In the simplest version of RCE, one typically ignores spherical geometry and places the flow in a doubly periodic domain in which the forcing and boundary conditions are all horizontally homogeneous. This allows the study of the interactions between radiation and moist convection in a simple geometry (e.g., Bretherton et al. 2005; Romps and Kuang 2010; Muller et al. 2011). In many cases, the flow is assumed to be nonrotating, but it is also very interesting to consider rotating radiative–convective equilibrium (RRCE) by using an *f*-plane geometry. In all simulations of RRCE documented to date, if the domain is large enough it fills up with long-lived tropical cyclones (TCs). With both the size and intensity of these TCs intrinsically determined, such an equilibrium provides an ideal framework to study equilibrated TCs and their dependence on large-scale parameters.

Previous studies of RRCE all prescribe a horizontally homogeneous sea surface temperature (SST) over the domain and thus neglect the response of SST to TCs (Held and Zhao 2008; Khairoutdinov and Emanuel 2013; Merlis et al. 2013; Shi and Bretherton 2014; Zhou et al. 2014; Reed and Chavas 2015; Ballinger et al. 2015; Merlis et al. 2016). It is, however, well known that TCs can induce substantial cooling at the surface along their paths (e.g., Price 1981), which in turn can have a profound impact on TC intensity (Bender et al. 1993; Bender and Ginis 2000; Zhu and Zhang 2006; Lin et al. 2013). Shen and Ginis (2003) shows that the surface cooling caused by TCs is dominated by the effect of internal ocean dynamics, mixing and upwelling, in the deep- and open-ocean regions but by surface fluxes in the near-coastal shallow-ocean regions. The quantitative impact of the surface cooling on TC intensity has been statistically studied by downscaling with a simple axisymmetric hurricane model (e.g., Emanuel 1999; Schade and Emanuel 1999; Vincent et al. 2014). The axisymmetric

[a] Current affiliation: Scripps Institution of Oceanography, University of California, San Diego, La Jolla, California.

Corresponding author e-mail: Wenyu Zhou, zhouwy1128@gmail.com

DOI: 10.1175/JAS-D-16-0195.1

hurricane model (Emanuel 1995) is based on the same assumptions as those that can eventually lead to the widely used TC potential intensity (Emanuel 1986, 1991). Particularly, the boundary layer is assumed to be well mixed. It is, however, not clear whether this assumption still holds when there is substantial surface cooling at the eyewall and how the effect of the surface cooling on TC intensity will be modified.

In this study, we achieve three-dimensional RRCE with column physics of the High Resolution Atmospheric Model (HiRAM) at GFDL, following the approach of Zhou et al. (2014), but with SST coupled to a simple slab ocean layer. The effect of coupling on TCs is then studied by varying the layer depth H. By using a simple slab ocean layer, only the effect from surface fluxes is included in the SST evolution. However, we feel that it is the natural place to start when approaching the problem of RRCE with interactive SST, especially because it is the simplest way to configure an energetically closed lower boundary condition.

With coupling to a slab ocean, the surface underneath the TC eyewall cools relative to the environment. But TCs are still able to sustain themselves in our simulations despite the cooling and irrespective of the depth of the slab. With strong surface cooling, the atmospheric boundary layer in the eyewall region is no longer well mixed in this model. The TC intensity reduction caused by the cooling is found to be much smaller than that estimated by a potential intensity, taking into account the surface cooling at the eyewall and assuming that moist entropy is well mixed along angular momentum surfaces within the boundary layer.

The paper is organized as follows: The model configuration and experiments are described in section 2. A general description of the simulation results is given in section 3. The physics controlling the surface cooling at the eyewall is studied in section 4. The variations of the intensity and structure of TCs with the surface cooling are investigated, respectively, in sections 5 and 6. Section 7 gives a summary with discussion.

2. Model configuration and experiments

RRCE can be investigated both with cloud-resolving models in which deep convection is partly resolved (Khairoutdinov and Emanuel 2013) and with the lower-resolution hydrostatic dynamics and column physics of a global comprehensive climate model (GCM) (Held and Zhao 2008; Zhou et al. 2014). Because of the limited computational power, cloud-resolving models are usually used to study a single TC in a small domain (e.g., Nolan et al. 2007; Brown and Hakim 2013; Tao and Zhang 2014; Zhou 2015; Davis 2015; Wing et al. 2016), although an artificially large Coriolis parameter can be used to produce multiple TCs even in a small domain (Khairoutdinov and Emanuel 2013). There is no such restriction for lower-resolution hydrostatic models using column physics from a GCM. Also, GCMs are one of the tools used to predict the impact of climate change on TC statistics, and they are moving toward higher resolution such that many aspects of their TC simulations are becoming more realistic (e.g., Knutson et al. 2010; Walsh et al. 2015; Camargo and Wing 2016). Being able to study these GCM-generated TCs in this idealized geometry, and eventually comparing them to analogous simulations at cloud-resolving resolutions, will help us understand the limitations and strengths of TC simulations in GCMs.

Here, we achieve RRCE by coupling the column physics of the HiRAM to rotating hydrostatic dynamics in a doubly periodic f plane. The uniform Coriolis parameter is set at a constant value of $5 \times 10^{-5}\,\mathrm{s}^{-1}$, corresponding to the latitude of 20°N. HiRAM's simulation of the observed global climatology and interannual variability of hurricane frequency is described in Zhao et al. (2009). The realism of the simulation is also discussed in Zhao et al. (2012), Shaevitz et al. (2014), and Walsh et al. (2015). The atmospheric model used in this study has 32 vertical levels with the lowest level at about 35 m and the top level at about 2 hPa. The horizontal resolution is 25 km. The GFDL interactive radiation scheme is used for radiative processes but with no diurnal or seasonal cycle. The incoming solar radiative flux uses an annual-mean zenith angle corresponding to the latitude of 35°N such that the simulated SST is close to the observed tropical-mean value. The cloud fraction is estimated by a simple diagnostic scheme assuming a subgrid-scale distribution of total water. A convection scheme originally developed for shallow convection (e.g., Bretherton et al. 2004; Zhao et al. 2009) is used to parameterize all convection, with entrainment rate optimized for the global simulation. Surface fluxes are computed using the Monin–Obukhov similarity theory, with a gustiness component of $1\,\mathrm{m\,s}^{-1}$. The vertical diffusion is handled by a K-profile scheme (Lock et al. 2000). In all of these respects, this column physics is identical to that described in Zhao et al. (2009). A large domain (8000 km × 8000 km) is used to allow multiple storms to exist simultaneously.

SST is predicted by coupling the atmosphere to a slab ocean model such that at each grid point we have

$$\frac{\partial \mathrm{SST}}{\partial t} = \frac{F_s}{\rho_w c_w H}, \tag{1}$$

where ρ_w and c_w are the density and heat capacity of water, H is the depth of the ocean layer, and F_s is the net surface energy flux into the ocean.

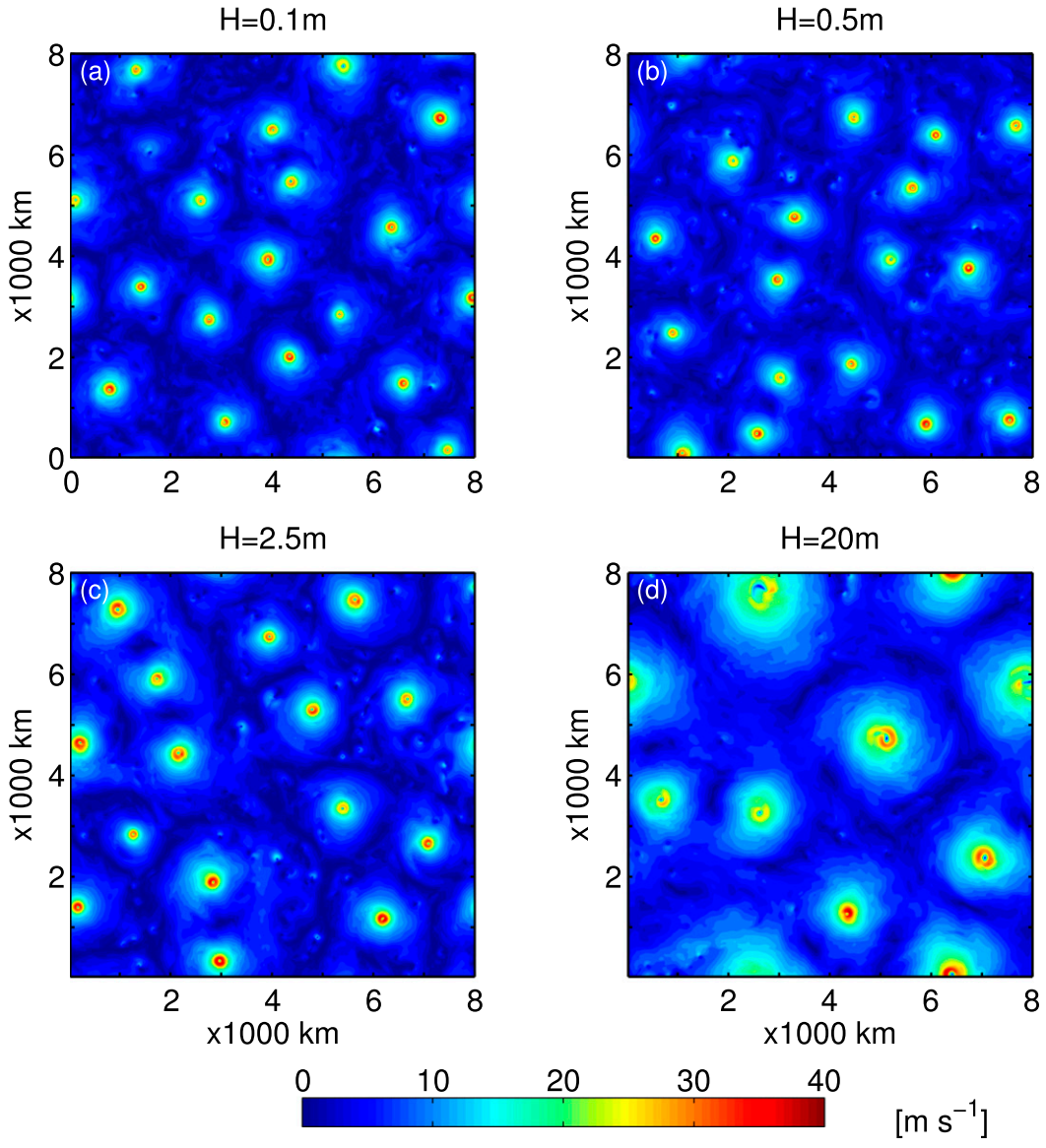

FIG. 1. Snapshots of instantaneous surface winds for simulations with H = (a) 0.1, (b) 0.5, (c) 2.5, and (d) 20 m.

The sensitivity of TCs to the underlying heat capacity is investigated by varying the depth H from 0.1 to 20 m. We first achieve an equilibrium with a layer depth of 1.25 m and then restart from this equilibrium for another 10 yr with different depths to reach full equilibria. For comparison, one additional simulation is conducted with fixed SST. The fixed SST is set at 296.35 K, a value obtained by extrapolating the simulated domain-mean SST expressed as a function of H^{-1} to very large H. Tropical cyclones are identified over the domain by finding points with surface pressure satisfying two criteria: 1) less than a critical value of 980 hPa and 2) a minimum at this point within the surrounding 10 grid × 10 grid box (250 × 250 km^2). TC statistics are computed using all TCs collected over the last 4 months of the simulations, if not otherwise stated.

3. Description

Figure 1 shows the snapshots of instantaneous surface winds in simulations with different H. Similar to RRCE with fixed SST, the domain still fills up with long-lived TCs that persist for months in all cases. TCs wander around because of the turbulent flow among them. The difference is that SST under the eyewall region of TCs is now cooler relative to that of the environment (Fig. 2). Figure 3 shows the azimuthal-mean height–radius cross sections of the horizontal temperature

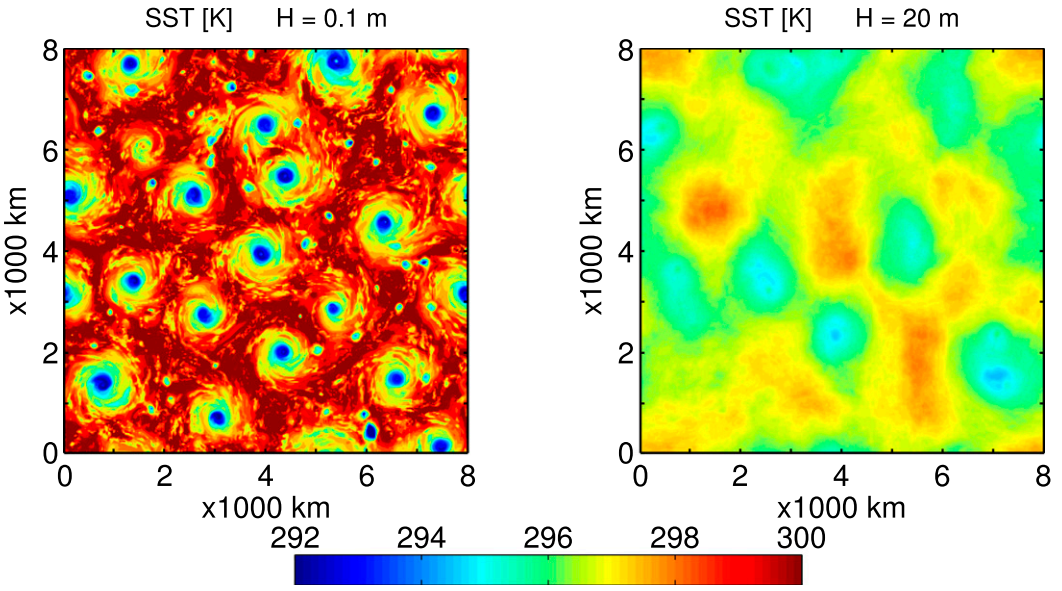

FIG. 2. Snapshots of instantaneous sea surface temperature for simulations with H = (left) 0.1 and (right) 20 m.

anomaly and velocity averaged over all collected TCs in simulations with H = 0.1 and 20 m. The cooling at the surface extends upward and produces a shallow cold core under the typical warm core of TCs, particularly for the case with H = 0.1 m (Figs. 3a,b). While a 25-km resolution is not adequate to resolve more detailed aspects of the tropical cyclone structure, a well-defined eyewall with deep ascent is apparent, as well as the characteristic inflow in the boundary layer and outflow in the upper troposphere (Figs. 3c,d). Evidently, tropical cyclones become broader as H increases, but there is no obvious difference in their maximum wind.

Figure 4a shows the radial distribution of the azimuthal-mean SST averaged over all collected TCs in simulations with different H. As H decreases, the environmental SST increases while the eyewall SST cools further. The magnitude of the SST cooling underneath the eyewall relative to the environment (ΔSST; hereinafter referred to as "eyewall cooling") increases as H decreases but eventually levels off at about 6.5 K as H approaches zero (Fig. 5). It is interesting that TCs are still able to sustain themselves in spite of this substantial eyewall cooling.

4. Eyewall cooling of tropical cyclones

Before we look into how this eyewall cooling affects TCs in sections 5 and 6, we first investigate what causes the eyewall cooling and how the magnitude is determined. As shown in Fig. 4b, the cooling in the eyewall region is related to the negative net surface energy flux there (the sign convention is that positive values are into and negative values are out of the ocean). The net surface flux can be decomposed into the radiative and turbulent heat flux components. For the radiative part, the surface receives less shortwave radiative flux and emits less longwave radiative flux (Fig. 4c) because of the excessive clouds in the eyewall region. The net effect is dominated by the shortwave part, leading to less net radiative flux received in the eyewall region. The surface also transfers more turbulent heat flux into the atmosphere because of the stronger surface winds there. But, as H decreases, surface turbulent heat flux is suppressed in the eyewall region (Fig. 4d) as the surface enthalpy disequilibrium decreases with cooler SST (Fig. 4e). To conclude, the negative surface energy flux originates from the shortwave cloud radiative effect and strong winds in the eyewall region but is also strongly offset by a negative SST–surface disequilibrium feedback. Particularly, the maximum magnitude of the negative surface flux decreases from about 200 W m^{-2} at H = 20 m to about 25 W m^{-2} at H = 0.5 m and eventually becomes zero as H approaches zero. As we will see, this decreasing trend allows the eyewall cooling to increase less rapidly and eventually level off as H decreases.

To better understand what controls the magnitude of the eyewall cooling, we develop a minimalist model, as described below. We start from the simplest case at the limit of H = 0 m. No energy is allowed to be stored in the ocean so that the surface energy balance equation for the environment and eyewall can be written respectively as

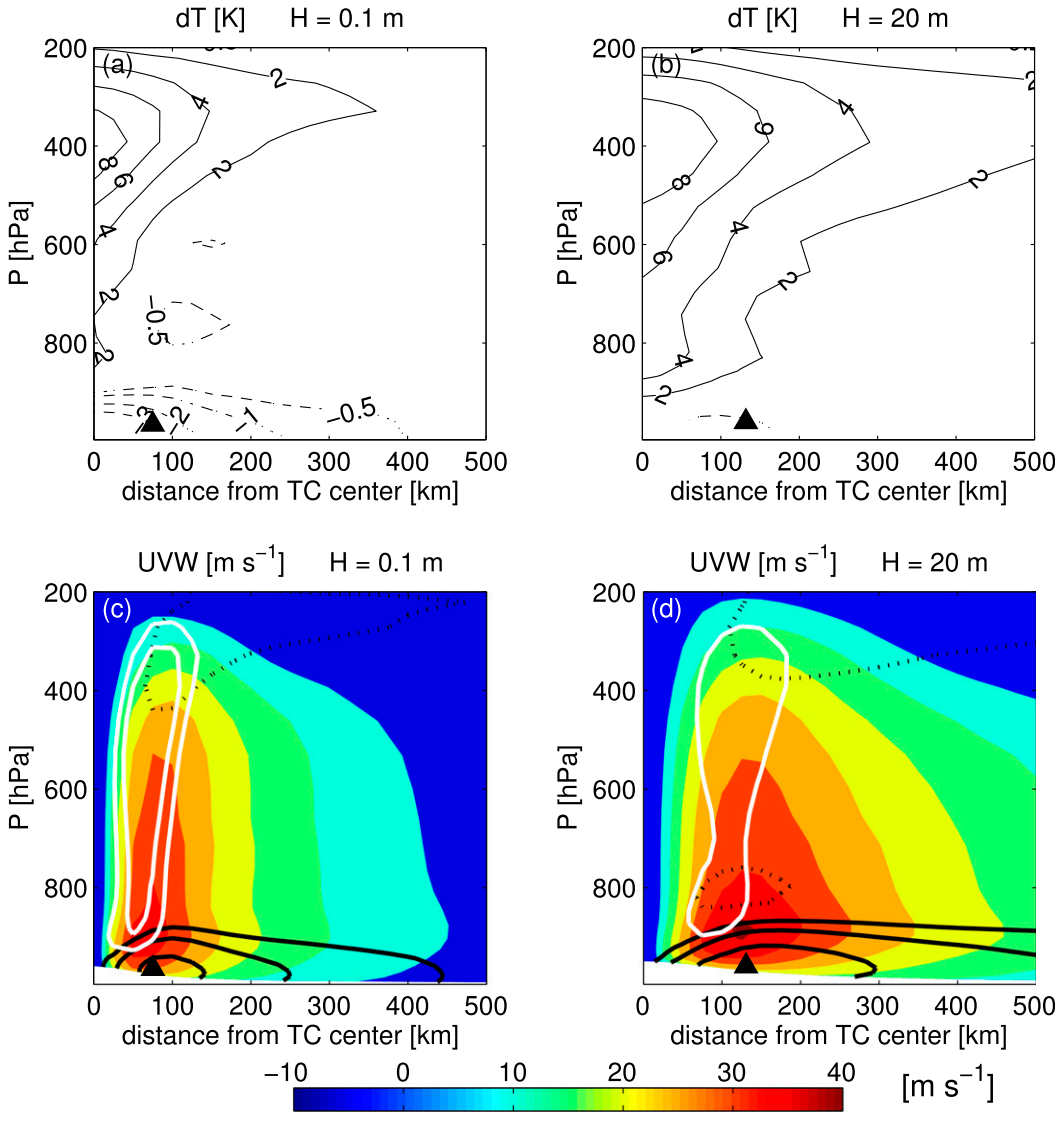

FIG. 3. Azimuthal-mean height–radius cross section of (a),(b) horizontal temperature anomaly relative to the horizontal mean and (c),(d) winds averaged over all collected TCs in simulations with H = (left) 0.1 and (right) 20 m. Tangential winds are shown by color shading. Radial winds (black contours) are contoured at 2, 5, 10, and 15 m s^{-1}. Positive (outflow) values are dotted; negative (inflow) values are solid. Vertical velocity (white contours) is contoured at 0.2 and 0.3 m s^{-1}. Black triangles indicate the radius of the maximum wind.

$$R_e = V_e C_k c_a \rho_a \delta k_e \quad \text{and} \tag{2}$$

$$R_c = V_c C_k c_a \rho_a \delta k_c, \tag{3}$$

where the subscripts e and c represent the environment and the eyewall, respectively, R is the downward net surface radiative flux, V is the surface wind speed, δk is the surface enthalpy disequilibrium (K), C_k is the surface exchange coefficient for enthalpy, and ρ_a and c_a are the density and heat capacity of air at constant pressure, respectively.

Combining the above two equations, δk_c is related to δk_e as

$$\delta k_c = \delta k_e \frac{R_c}{R_e} \frac{V_e}{V_c}. \tag{4}$$

We can see the radiative effect of clouds is represented by the term R_c/R_e, while the effect of strong winds is represented by the term V_e/V_c. Both terms reduce δk_c and thus SST$_c$. In our simulation, both R_c/R_e and V_e/V_c are close to zero (Figs. 4c,h). This leads to

$$\delta k_c \simeq 0. \tag{5}$$

That is, the surface disequilibrium needs to be nearly zero at the eyewall as H approaches zero, which is

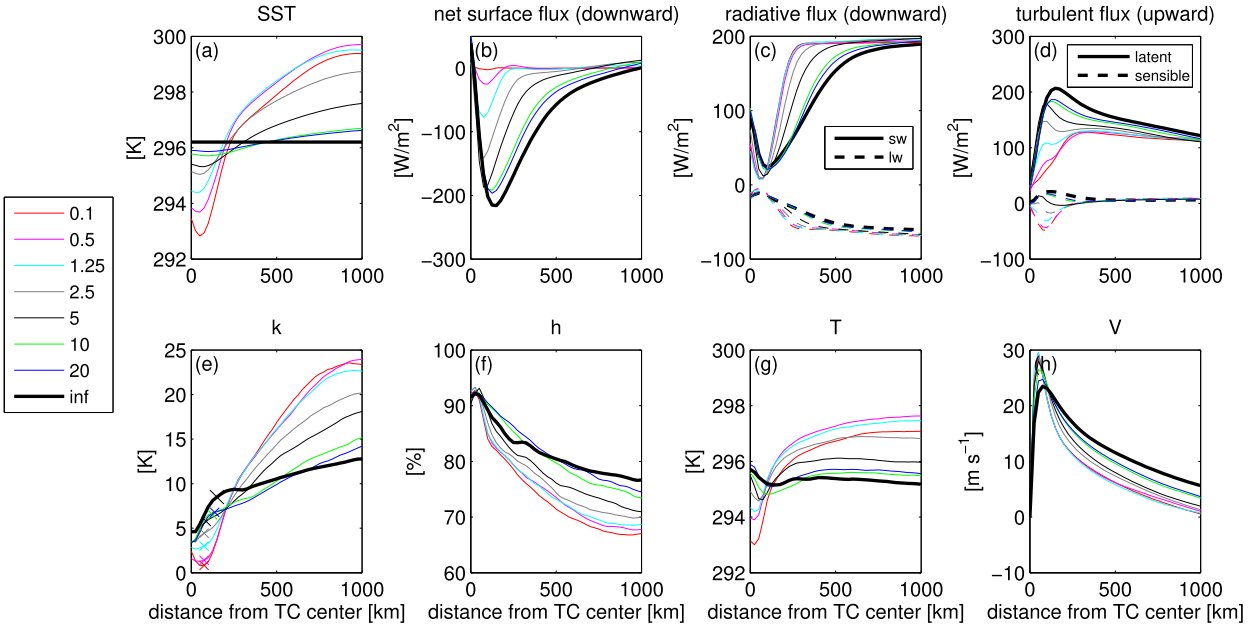

FIG. 4. Azimuthal-mean (a) SST, (b) net surface energy flux (positive downward), (c) net shortwave (solid) and longwave (dashed) fluxes (positive downward), (d) latent (solid) and sensible (dashed) heat flux (positive upward), (e) surface disequilibrium k, (f) surface relative humidity h, (g) surface air temperature T, and (h) surface tangential wind speed V as a function of the distance from TC center averaged over all collected TCs in simulations with different H. The cross symbols in (e) indicate the radius of the maximum wind.

consistent with the simulation results, as shown in Fig. 4e.

On the other hand, given the definition of the surface disequilibrium

$$\delta k_e \equiv \mathrm{SST}_e - T_e + L_v/c_a[q^*(\mathrm{SST}_e) - h_e q^*(T_e)] \quad \text{and}$$
$$\delta k_c \equiv \mathrm{SST}_c - T_c + L_v/c_a[q^*(\mathrm{SST}_c) - h_c q^*(T_c)],$$

one can formulate δk_c alternatively as

$$\delta k_c = \delta k_e - (\Delta\mathrm{SST} - \Delta T + \alpha\Delta\mathrm{SST} - h_e\alpha\Delta T) - L_v/c_a q^*(T_c)\Delta h, \tag{6}$$

where the symbol Δ represents the difference between the environment and the eyewall, T and h are the surface air temperature and relative humidity, respectively, and q^* is the saturation vapor pressure. The parameter $\alpha = (L_v^2 q^*)/(c_a R_v T^2) \simeq 2.8$ represents the mean sensitivity of saturation vapor pressure to temperature for a range of SST from 294.5 to 299.5 K (Fig. 4a).

As shown in Fig. 6a, ΔT is found to be roughly proportional to ΔSST with a ratio of 0.5. Developing a theory for this ratio would involve the energy balance of the atmospheric mixed layer as well as the oceanic slab, so we take advantage of it being roughly constant across our simulations and simplify it to a fixed value. Using $\Delta T = \xi\Delta\mathrm{SST}$, the above equation can be simplified as

$$\delta k_c = \delta k_e - \Lambda\Delta\mathrm{SST} - \eta. \tag{7}$$

The parameter $\Lambda = 1 - \xi + \alpha - \xi\alpha h_e \simeq 2.3$ represents the strength of the SST–surface disequilibrium feedback as a combined result of both SST and T variation, estimated based on a ratio $\xi = 0.5$ and a mean environmental relative humidity $h_e = 0.75$ (Fig. 4f). The parameter

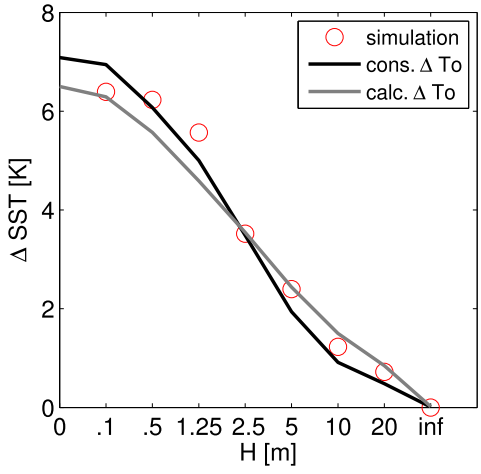

FIG. 5. The surface eyewall cooling relative to the environment averaged over all collected TCs in simulations with different ocean-layer depth (ΔSST; red circles) and estimated by Eq. (12) using a constant $\Delta\mathrm{SST}_o = 6.5$ K (gray line) and calculated $\Delta\mathrm{SST}_o$ from simulated δk_e (black line).

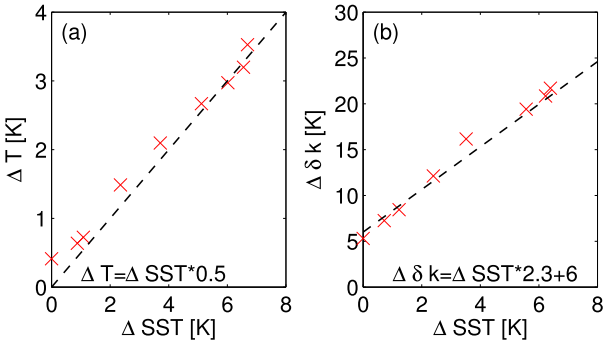

FIG. 6. (a) Relationship between ΔSST (SST difference between the eyewall and the environment) and ΔT (near-surface air temperature difference between the eyewall and the environment). (b) Relationship between ΔSST and $\Delta\delta k$ (surface disequilibrium between the eyewall and the environment). The dashed lines represent linear relationships indicated by the equations shown in the panels.

$\eta = L_v/c_a q^*(T_c)\Delta h \simeq 6$ measures the difference in disequilibrium $\Delta\delta k$ caused by the different relative humidities Δh between the eyewall and the environment, estimated based on a mean $\Delta h \simeq 0.15$ (Fig. 4f) and $T_c \simeq 294.5$ K (Fig. 4g). As shown in Fig. 6b, Eq. (7) captures the relationship between ΔSST and $\Delta\delta k = \delta k_e - \delta k_c$ in our simulations.

Combining Eqs. (5) and (7) provides an estimate for ΔSST at the limit of zero H as

$$\Delta\mathrm{SST} \simeq \frac{\delta k_e - \eta}{\Lambda}. \tag{8}$$

Using $\Delta k_e \simeq 22$ K from the $H = 0.1$-m case as shown in Fig. 4e, the above equation gives an estimate of ΔSST of 7 K. This is very close to what we see in our simulation as H approaches zero (Fig. 5). This derivation indicates that the eyewall cooling has a well-defined value even at the limit of zero H and that this value is not directly dependent on the TC intensity.

Next, we would like to address the effect of the finite H on the eyewall cooling by considering the competition between the relaxation of SST to the $H = 0$-m limit and the restoring tendency due to the propagation of the storm into regions of warmer SST. In the reference frame following a TC, one can think of a flow in the stagnant slab ocean in the opposite direction to the translation of the TC. This flow transports energy from the environment, which is heated by the positive net surface flux, into the cold pool of TCs, which is cooled by the negative net surface flux. Given a typical value for this storm drift and the size of the cold pool, there is a characteristic time scale τ for the storm to escape from its cold SSTs. The energy transport effect due to this drift can then be approximated as

$$\rho_w H c_w \frac{\Delta\mathrm{SST}}{\tau}. \tag{9}$$

One can then rewrite Eq. (3) by including this effect into the surface energy balance equation at the eyewall:

$$R_c + \rho_w H c_w \frac{\Delta\mathrm{SST}}{\tau} = V_c C_k c_a \rho_a \delta k_c. \tag{10}$$

By combining Eqs. (2) and (10), and given that $R_c V_e / R_e V_c \simeq 0$ as seen in Fig. 4c, we get

$$\delta k_c \simeq \mu \frac{H}{\tau V_c} \Delta\mathrm{SST}, \tag{11}$$

where

$$\mu = \frac{1}{C_k}\frac{\rho_w}{\rho_a}\frac{c_w}{c_a} \simeq 4 \times 10^5.$$

Different from $\delta k_c \simeq 0$ at the limit of $H = 0$, the finite slab ocean leads to a positive surface disequilibrium at the eyewall.

Substituting Eq. (11) into Eq. (7), we obtain a relationship between ΔSST and H as

$$\Delta\mathrm{SST} = \frac{\Delta\mathrm{SST}_o}{1 + H/H_o}, \tag{12}$$

where

$$\Delta\mathrm{SST}_o = \frac{\delta k_e - \eta}{\Lambda}, \quad \text{and} \tag{13}$$

$$H_o = \frac{\Lambda}{\mu} V_c \tau. \tag{14}$$

Setting τ proportional to $\mathscr{L}/\mathscr{V}$, where $\mathscr{L}$ is a characteristic length scale of the storm-induced cooling and $\mathscr{V}$ is a typical storm translation speed, then $H_o \sim \mathscr{L} V_c/\mathscr{V}$. Therefore, ΔSST increases approaching $\Delta\mathrm{SST}_o$ more closely, as the ratio of the storm intensity V_c to $\mathscr{V}$ increases. As shown in Fig. 5, this formula estimates the variation with H fairly well by assuming a constant $\Delta\mathrm{SST}_o \simeq 6.5$ K and $H_o \simeq 3$ m given the values of α, Λ, and η listed above and setting $V_c = 30\,\mathrm{m\,s^{-1}}$ and $\tau = 2$ days. The value $\Delta\mathrm{SST}_o \simeq 6.5$ K corresponds to a mean δk_e of 20 K. We determine τ from this fit rather than trying to estimate it directly from the simulations. It is unclear how one would develop a theory for τ or $\mathscr{V}$ for an RRCE model.

We note that $\Delta\mathrm{SST}_o$ varies with H in these simulations, since δk_e increases as H decreases (Fig. 4e). The enhanced δk_e with decreased H can be interpreted as a mechanism to maintain the similar strength of surface flux in order to balance with radiative cooling in the presence of weaker environmental surface wind (Fig. 4h). This enhanced δk_e is achieved through increased environmental SST (Fig. 4a) and decreased environmental relative humidity (Fig. 4f).

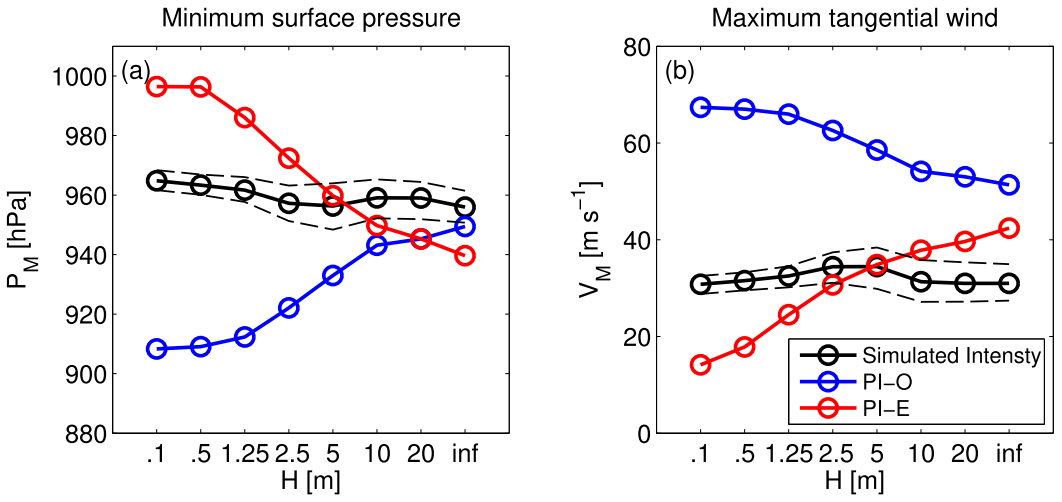

FIG. 7. Intensity and PIs as a function of H. The black solid lines show the median intensity of all collected TCs, and the gray dashed lines indicate the first and third quartiles. The blue lines show PI computed from the original algorithm (PI-O). The red lines show PI computed from the modified PI algorithm considering the eyewall cooling (PI-E).

Using $\Delta\mathrm{SST}_o$ computed from δk_e in the simulations [Eq. (13)] gives a slightly better fit (Fig. 5).

5. Intensity of tropical cyclones

Now we move on to the impact of the eyewall cooling on the intensity of TCs. Figure 7 shows the mean minimum surface pressure and maximum surface wind of all collected TCs in simulations with different H. Despite the substantial eyewall cooling, TC intensity barely decreases as H decreases in our simulations (Fig. 7). This is surprising since it is well established based on both observations and models that the cooling of SSTs by air–sea coupling can reduce TC intensity dramatically (e.g., Bender et al. 1993; Schade and Emanuel 1999; Zhu and Zhang 2006; Lin et al. 2013; Vincent et al. 2014).

We first try to understand our simulation results from the potential intensity (PI) theory of tropical cyclones (Emanuel 1991; Bister and Emanuel 2002; Garner 2014), which estimates the maximum TC intensity that can be achieved in a given large-scale environment as follows:[1]

$$R\overline{T_{ve}}\ln\left(\frac{P_e}{P_c}\right) = \mathrm{CAPE}_c - \mathrm{CAPE}_e + \beta(\mathrm{CAPE}_c^* - \mathrm{CAPE}_c) \quad \text{and} \tag{15}$$

$$V_{\mathrm{PI}}^2 = 2\beta(\mathrm{CAPE}_c^* - \mathrm{CAPE}_c). \tag{16}$$

The original algorithm (Bister and Emanuel 2002) assumes that surface conditions (SST, air temperature, and relative humidity) are the same between the outer eyewall and the environment. The values of CAPE_c and CAPE_c^* are then computed from the environmental profile as follows:[2]

$$\mathrm{CAPE}_c(P^e, T^e, \mathrm{RH}^e; P_c, T_s^e, \mathrm{RH}_s^e) \quad \text{and} \tag{17}$$

$$\mathrm{CAPE}_c^*(P^e, T^e, \mathrm{RH}^e; P_c, \mathrm{SST}^e). \tag{18}$$

The result computed using the original algorithm[3] is shown in Fig. 7 by blue circles, which indicate an increase in intensity with decreasing H as measured either by minimum pressure or maximum winds. The increasing intensity with decreasing H reflects the increasing surface disequilibrium in the environment (Fig. 4e).

[1] Here, R is the ideal gas constant, P_e is the environmental surface pressure, and P_c is the potential minimum pressure at the outer eyewall; $\overline{T_{ve}}$ is the mean environmental virtual temperature between the surface and $P = P_c$, $\beta = C_k T_b / 2C_d T_o$, where C_k and C_d are exchange coefficients for energy and momentum and T_b and T_o are the inflow and outflow temperature, respectively. The environmental convective available potential energy is CAPE_e CAPE_c and CAPE_c^* refer to the hurricane CAPE, which is defined by the potential energy of a parcel lifted from the outer eyewall surface pressure; CAPE_c is associated with the surface air parcel and CAPE_c^* is associated with the saturated parcel at SST.

[2] Here, P^e, T^e, and RH^e are the environmental vertical profiles of pressure, temperature, and relative humidity, respectively; SST^e, T_s^e, and RH_s^e are the environmental SST, surface air temperature, and surface relative humidity, respectively, and P_c is then interactively computed from the above equations.

[3] We use the iterative algorithm as in ftp://texmex.mit.edu/pub/emanuel/TCMAX/ and assume a ratio of drag coefficients $C_k/C_d = 0.7$ and the pseudoadiabatic ascent.

To account for the effect of the eyewall cooling, we modify this algorithm by using the simulated SST at the radius of the maximum wind (SST^c) for $CAPE^*_c$ and the simulated surface air temperature and relative humidity at the radius of maximum wind (T_s^c, RH_s^c) for $CAPE_c$:

$$CAPE_c(P^e, T^e, RH^e; P_c, T_s^c, RH_s^c) \quad \text{and} \tag{19}$$

$$CAPE^*_c(P^e, T^e, RH^e; P_c, SST^c). \tag{20}$$

We note that a similar approach has been used in Lin et al. (2013) and Huang et al. (2015) to build a modified potential intensity that accounts for the ocean coupling. The difference here is that in their method the surface air temperature and relative humidity are still assumed to be the same as those of the environment, and only the difference in SST is considered. There is, however, considerable difference in both the surface air temperature and relative humidity between the eyewall and the environment in our simulations (Fig. 4f and 4g). As indicated in Fig. 7 by red circles, our modified algorithm predicts a reduction in intensity with decreasing H, consistent with the decreasing surface disequilibrium at the eyewall, as we have seen in Fig. 4e.

However, the simulated intensity dependence on H is surprisingly flat. This means that the simulated TC intensity reduction caused by the eyewall cooling is much smaller than that predicted by PI. The flatness of TC intensity as a function of H is roughly consistent with the fact that the warm core temperature is not very different in the small and large H cases (Fig. 3), although the warm core is smaller for small H, as discussed in the following section. It appears that the surface cooling condition is not exported into the interior with the boundary layer inflow passing over the cold pool (Fig. 3). PI is founded on independent relationships between moist entropy S and angular momentum M arising from free-trajectory conservation and dynamical balances

$$\left.\frac{dS}{dM}\right|_b = -\frac{V_b}{(T_b - T_o)r} \tag{21}$$

on the one hand[4] and the well-mixed boundary layer transformations via surface fluxes

$$\left.\frac{dS}{dM}\right|_b = \frac{\overline{dS}}{dM} = -\frac{C_k}{C_d}\frac{k^* - k}{rT_sV} \tag{22}$$

on the other hand.[5]

This leads to the well-known analytical formula of PI as

$$V_{PI} \simeq \sqrt{\frac{C_k}{C_d}\frac{T_b - T_o}{T_s}(k^* - k)}. \tag{23}$$

The azimuthal-mean height–radius cross sections of moist entropy and angular momentum are shown in Fig. 8 for simulations with $H = 0.1$ and 20 m. It is found that, in the case with substantial eyewall cooling, moist entropy is not well mixed along angular momentum surfaces in the boundary layer, one should instead have

$$V = \lambda V_{PI}, \tag{24}$$

where

$$\lambda = \sqrt{\left.\frac{dS}{dM}\right|_b \Big/ \frac{\overline{dS}}{\overline{dM}}} \tag{25}$$

is the parameter measuring how well moist entropy is mixed along angular momentum surfaces in the boundary layer. Given that dS/dM decreases from the small negative value at the surface to the large negative value at the boundary layer top (Fig. 8), the parameter λ is larger than 1. According to Eq. (24), this helps explain the stronger TC intensity in our simulations compared to what PI predicts. From this perspective, there could be sensitivity of these results to the boundary layer formulation. A boundary layer scheme that favors the decoupling between the storm interior and the cooler surface will reduce the influence of the surface cooling on TC intensity. There may also be a distinction between RRCE, with nearly stationary storms having time to arrange their structure to avoid their cold eyewall SSTs, and more realistic scenarios of mature storm–SST interactions where cold SSTs impact storm intensity more substantially.

[4] Here, V_b and T_b are the azimuthal wind speed and temperature at the top of the boundary layer, respectively, and T_o is the outflow temperature along an angular momentum surface where it passes through the point of $V = 0$.

[5] Here, $\bar{s}$ and $\overline{M}$ are the entropy and angular momentum averaged through the depth D of the boundary layer, respectively, C_k and C_d are exchange coefficients for energy and momentum, respectively, $|\mathbf{V}|$ is the wind speed at the flux reference level, V is the azimuthal velocity, and $k^* - k$ is the surface disequilibrium of enthalpy. The turbulent flux of entropy through the top of the boundary layer and the entropy source from dissipative heating have been neglected.

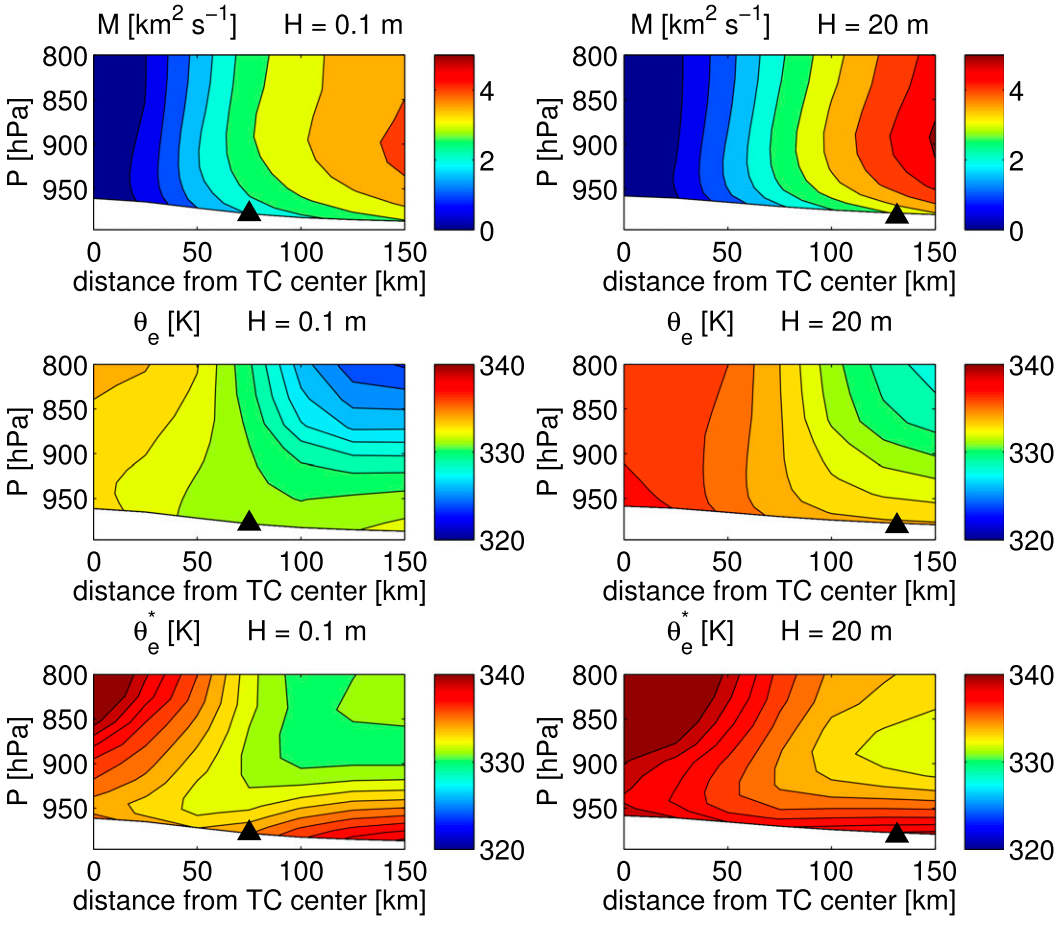

FIG. 8. Azimuthal-mean height–radius cross section of (top) angular momentum ($m^2 s^{-1}$), (middle) equivalent potential temperature (K), and (bottom) saturated equivalent potential temperature (K) in the boundary layer averaged over all collected TCs in simulations with H = (left) 0.1 and (right) 20 m. Black triangles indicate the radius of the maximum wind.

Besides the potential intensity theory, the entropy budget provides a different perspective to study TC intensity in RRCE (Khairoutdinov and Emanuel 2013). By assuming the dynamical dissipation is dominated by the friction in the boundary layer, one can write the domain-mean entropy balance as

$$\overline{\rho_a C_d V^3} \simeq \varepsilon \overline{Q}, \tag{26}$$

where ε measures the thermodynamic efficiency of RRCE, Q is the radiative cooling rate, and the overline means domain mean.

In our simulations, $\overline{Q}$, as indicated by the domain-mean precipitation rate, is nearly constant as H is varied (Fig. 9a). If the thermodynamic efficiency is also roughly independent of H and if we can assume that the domain-mean intensity power $\overline{V^3}$ is proportional to the cubed TC intensity V_M^3, then the entropy budget provides an explanation for the constancy of the TC intensity as H is varied. However, as shown in Fig. 9b, the efficiency is not constant with H, but in fact increases with increasing H by an amount that in itself would generate a 30% change in intensity. If the efficiency of RRCE was near its thermodynamic limit determined by the fractional temperature difference across the troposphere, we might expect it to be independent of H, but, in fact, we find much smaller efficiencies [$\varepsilon \simeq 0.02 < (T_s - T_o)/T_s \simeq 0.1$, where the effective radiative temperature $T_o \simeq 270$ K], which are comparable to those found in nonrotating RCE (Pauluis and Held 2002a,b). Whether this result is model dependent remains to be seen. The intensity changes that would result from these changes in efficiency seem to be balanced by changes in storm structure. As H increases, the TC structure changes such that the ratio between the radius of the maximum wind R_{MW} and the size of TC, L, increases (Fig. 9c). This leads to a larger contribution from the maximum wind V_M on the

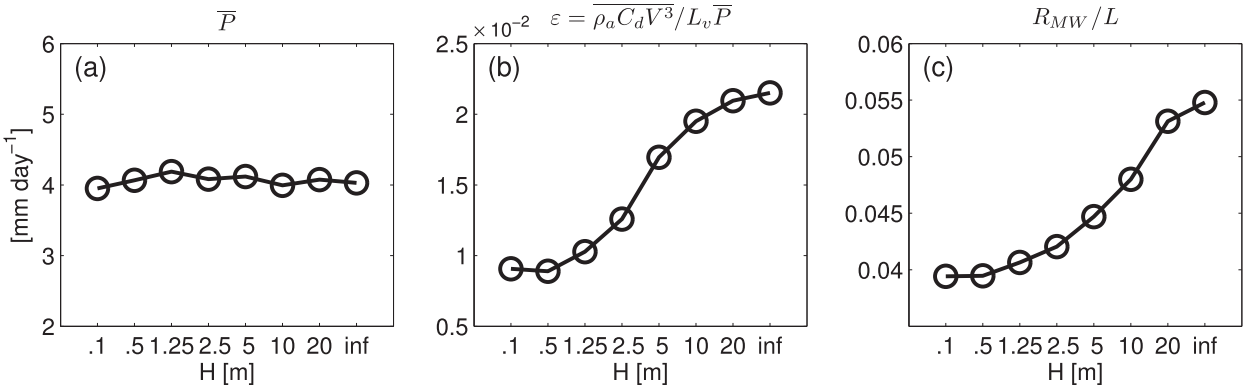

FIG. 9. (a) Domain-mean precipitation rate $\overline{P}$, (b) the thermodynamic efficiency ε, and (c) the ratio between the radius of the maximum wind R_{MW} and the size of TCs L.

average intensity V and thus a larger ratio of $\overline{V^3}/V_M^3$, which offsets the effect of the increasing efficiency on the TC intensity.

6. Structure of tropical cyclones

As is clear from the snapshots shown in Figs. 1 and 2, the spacing between storms decreases as H is reduced. To give a quantitative estimate, we compute the average spacing as $L \sim \sqrt{A/n}$, where A is the domain area and n is the time-mean TC number within the domain. This is the scale over which a cyclone suppresses others. It is larger than a scale determined by the radius of a particular azimuthal wind speed (e.g., Chavas and Emanuel 2014). As shown in Fig. 10a, L decreases from $H = 20$ to 1.25 m and stays nearly constant as H further decreases. Two theoretical scalings for the size of TCs are compared to the simulation results. One is the Rossby radius of deformation $N\mathscr{H}/f$, where N is the static stability parameter and $\mathscr{H}$ is the scale height of the atmosphere. The other is the storm-related length scale $L \sim V_M/f$, where V_M is the maximum wind. Both scalings fail to capture the variation of L with H (not surprisingly), because the changes in mean tropospheric static stability are modest in these simulations and because the storm intensity is also nearly independent of H. Figure 10b shows the mean radius of the maximum wind R_{MW} defined using the azimuthally averaged surface wind from each storm and then averaged over all storms. The value of R_{MW} decreases continuously from $H = 20$ to 1.25 m

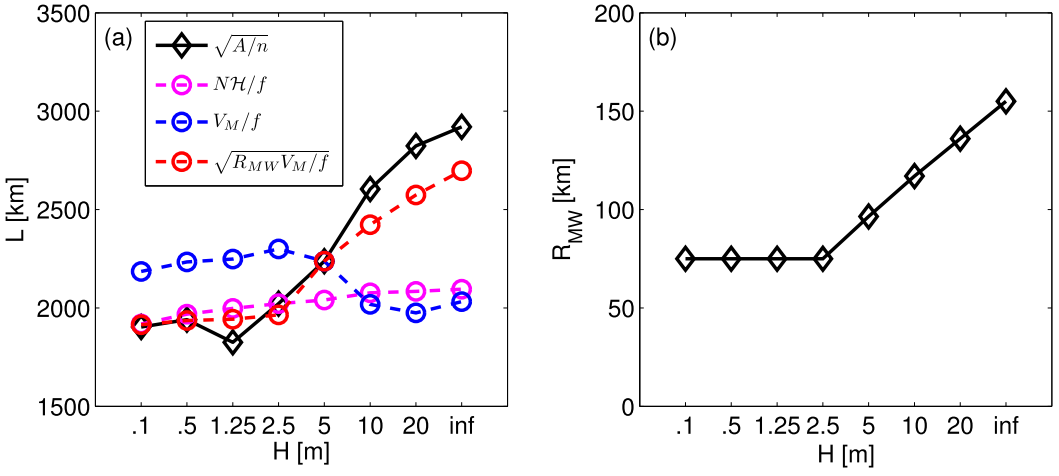

FIG. 10. (a) The size of TCs calculated as $L = \sqrt{A/n}$ (solid black line), Rossby radius of deformation $\sqrt{N\mathscr{H}/f}$ (pink line), the scaling of $\sqrt{V_M/f}$ (blue line), and $\sqrt{R_{MW}V_M/f}$ (red line). The stratification stability is calculated as $N^2 = (g/\theta_o)(\delta\theta/\delta z)$, where θ_o is the domain-mean potential temperature at 500 hPa and $\delta\theta$ and δz are the difference in the domain-mean potential temperature and height between 250 and 900 hPa. The scaling height of atmosphere $\mathscr{H}$ is set as a constant of 8 km. (b) The variation of the mean radius of the maximum wind R_{MW} as a function of H.

and stays nearly unchanged as H further decreases. The smaller R_{MW} with smaller H is also evident in Fig. 3.

Zhou et al. (2014) show that the relationship $L \sim \sqrt{R_{MW} V_M / f}$ works rather well in RRCE with fixed SST when parameters such as the rotation rate or SST are varied. As shown in Fig. 10a, this relationship holds up fairly well in these coupled SST simulations as H is varied. Although this relationship between L and R_{MW} itself is not a theory for L or R_{MW}, it implies that L and R_{MW} are highly correlated. A similar relation between R_{MW} and L is also theoretically derived in Emanuel and Rotunno (2011) and can be thought of as assuming a constant reduction factor of angular momentum from the environment to R_{MW}.

The constant R_{MW} with very small H is plausibly an artifact of the model resolution since it would be impossible to resolve storm structure on scales comparable to or smaller than the model's 25-km resolution. Assuming that the relation between L and R_{MW} is robust, the result that L also asymptotically approaches a constant at small H could also be an artifact of inadequate resolution. Putting side these small-H cases, we believe that the overall result that the storm scale contracts with decreasing H is likely to be robust to changing resolution, but the resolution and model sensitivity of this result and others described above will have to be tested in the future.

The reduction in R_{MW} and L with decreasing H is interesting, given TC intensity does not change much, as previous studies indicate that TC size is scaled with its intensity in RRCE with fixed SST (Khairoutdinov and Emanuel 2013; Chavas and Emanuel 2014). The decreasing SST at the eyewall may play a role, but we currently have no satisfactory explanation.

7. Conclusions

In this study, rotating radiative–convective equilibrium (RRCE) with coupled SST is achieved by coupling the column physics of GFDL's HiRAM model to rotating hydrostatic dynamics in a large doubly periodic domain. Unlike previous studies that prescribe a homogeneous fixed SST over the domain, SSTs are now predicted by coupling the atmosphere to a simple slab ocean layer. The sensitivity of TCs to the coupling is then investigated by varying the slab ocean depth H in a wide range.

With coupled SST, the eyewall region of TCs becomes cooler relative to the environment, as expected. This cooling originates from the strong winds and excessive clouds at the eyewall but is also strongly offset by a negative SST–surface disequilibrium feedback. The magnitude of the eyewall cooling increases as H decreases but levels off eventually at about 6.5 K as H approaches zero. A minimalist model suggests the form of $\Delta\mathrm{SST} \simeq \Delta\mathrm{SST}_o/(1 + H/H_o)$ for the dependence of this cooling on H.

TCs are still able to sustain themselves, even in cases with substantial eyewall cooling. In fact, we find only small variations of the mean TC intensity with changing H. The predictions of potential intensity theory are dependent on the assumptions regarding the properties of the atmosphere emerging from the boundary layer at the eyewall. The theory underestimates TC intensity in cases with substantial eyewall cooling, consistent with the small surface thermodynamic disequilibrium at the eyewall. We find that the boundary layer inflow in the simulated storms evades the shallow cold pool, and the storm interior is decoupled from the surface. The moist entropy is no longer well mixed along angular momentum surfaces in the boundary layer, as assumed in the potential intensity theory, and the reduction effect of TC intensity caused by the surface cooling is strongly reduced. This picture suggests that there may be sensitivity to the boundary layer parameterization in these results on the relationship between intensity and H. It is also worth noting that the coarse-resolution model replies on a convection scheme. Despite the scheme being optimized to produce a realistic global TC simulation, it may not fully capture the complex nature of the real moist convection and potentially cause biases in our simulations. Future analogous studies using high-resolution models are desired to further validate our results.

The horizontal scale of TCs in this model, as measured by the average spacing between storms or by the radius of the maximum wind, contracts as H decreases over most of the range of H simulated, except for the smallest H and the smallest storm scales, for which the results are presumed to be sensitive to the model resolution. Please note that this contraction occurs without the variation in TC intensity. The reason for this contraction as H decreases remains obscure.

There are other interesting properties of these simulated climates, such as domain-averaged cloud feedbacks and the associated climate sensitivity and changes in domain-averaged or environmental lapse rates and surface enthalpy disequilibrium, that we have not addressed here, choosing to focus on TC statistics instead. But, given the dominance of TCs in these RRCE simulations, it is likely that any understanding of how these other statistics of interest change as a function of the depth of the slab will require a fuller understanding of changes in TC statistics.

Acknowledgments. The authors thank Ming Zhao and Shian-Jiann Lin for making HiRAM available.

We also thank Bruce Wyman for his work in configuring the doubly periodic model. Wenyu Zhou is partly supported by the U.S. Department of Energy under Award DE-SC0006841 and partly by National Oceanic and Atmospheric Administration (NOAA) Cooperative Institute for Climate Science under Award NA08OAR4320752.

REFERENCES

Ballinger, A. P., T. M. Merlis, I. M. Held, and M. Zhao, 2015: The sensitivity of tropical cyclone activity to off-equatorial thermal forcing in aquaplanet simulations. *J. Atmos. Sci.*, **72**, 2286–2302, doi:10.1175/JAS-D-14-0284.1.

Bender, M. A., and I. Ginis, 2000: Real-case simulations of hurricane–ocean interaction using a high-resolution coupled model: Effects on hurricane intensity. *Mon. Wea. Rev.*, **128**, 917–946, doi:10.1175/1520-0493(2000)128<0917:RCSOHO>2.0.CO;2.

——, ——, and Y. Kurihara, 1993: Numerical simulations of tropical cyclone–ocean interaction with a high-resolution coupled model. *J. Geophys. Res.*, **98**, 23 245–23 263, doi:10.1029/93JD02370.

Bister, M., and K. A. Emanuel, 2002: Low frequency variability of tropical cyclone potential intensity 2. Climatology for 1982–1995. *J. Geophys. Res.*, **107**, ACL 5-1–ACL 5-4, doi:10.1029/2001JD000780.

Bretherton, C. S., J. R. McCaa, and H. Grenier, 2004: A new parameterization for shallow cumulus convection and its application to marine subtropical cloud-topped boundary layers. Part I: Description and 1D results. *Mon. Wea. Rev.*, **132**, 864–882, doi:10.1175/1520-0493(2004)132<0864:ANPFSC>2.0.CO;2.

——, P. N. Blossey, and M. Khairoutdinov, 2005: An energy-balance analysis of deep convective self-aggregation above uniform SST. *J. Atmos. Sci.*, **62**, 4273–4292, doi:10.1175/JAS3614.1.

Brown, B. R., and G. J. Hakim, 2013: Variability and predictability of a three-dimensional hurricane in statistical equilibrium. *J. Atmos. Sci.*, **70**, 1806–1820, doi:10.1175/JAS-D-12-0112.1.

Camargo, S. J., and A. A. Wing, 2016: Tropical cyclones in climate models. *Wiley Interdiscip. Rev.: Climate Change*, **7**, 211–237, doi:10.1002/wcc.373.

Chavas, D. R., and K. Emanuel, 2014: Equilibrium tropical cyclone size in an idealized state of axisymmetric radiative–convective equilibrium. *J. Atmos. Sci.*, **71**, 1663–1680, doi:10.1175/JAS-D-13-0155.1.

Davis, C. A., 2015: The formation of moist vortices and tropical cyclones in idealized simulations. *J. Atmos. Sci.*, **72**, 3499–3516, doi:10.1175/JAS-D-15-0027.1.

Emanuel, K. A., 1986: An air–sea interaction theory for tropical cyclones. Part I: Steady-state maintenance. *J. Atmos. Sci.*, **43**, 585–604, doi:10.1175/1520-0469(1986)043<0585:AASITF>2.0.CO;2.

——, 1991: The theory of hurricanes. *Annu. Rev. Fluid Mech.*, **23**, 179–196, doi:10.1146/annurev.fl.23.010191.001143.

——, 1995: The behavior of a simple hurricane model using a convective scheme based on subcloud-layer entropy equilibrium. *J. Atmos. Sci.*, **52**, 3960–3968, doi:10.1175/1520-0469(1995)052<3960:TBOASH>2.0.CO;2.

——, 1999: Thermodynamic control of hurricane intensity. *Nature*, **401**, 665–669, doi:10.1038/44326.

——, and R. Rotunno, 2011: Self-stratification of tropical cyclone outflow. Part I: Implications for storm structure. *J. Atmos. Sci.*, **68**, 2236–2249, doi:10.1175/JAS-D-10-05024.1.

Garner, S., 2014: The relationship between hurricane potential intensity and CAPE. *J. Atmos. Sci.*, **72**, 141–163, doi:10.1175/JAS-D-14-0008.1.

Held, I. M., and M. Zhao, 2008: Horizontally homogeneous rotating radiative–convective equilibria at GCM resolution. *J. Atmos. Sci.*, **65**, 2003–2013, doi:10.1175/2007JAS2604.1.

Huang, P., I.-I. Lin, C. Chou, and R.-H. Huang, 2015: Change in ocean subsurface environment to suppress tropical cyclone intensification under global warming. *Nat. Commun.*, **6**, 7188, doi:10.1038/ncomms8188.

Khairoutdinov, M., and K. Emanuel, 2013: Rotating radiative-convective equilibrium simulated by a cloud-resolving model. *J. Adv. Model. Earth Syst.*, **5**, 816–825, doi:10.1002/2013MS000253.

Knutson, T. R., and Coauthors, 2010: Tropical cyclones and climate change. *Nat. Geosci.*, **3**, 157–163, doi:10.1038/ngeo779.

Lin, I.-I., and Coauthors, 2013: An ocean coupling potential intensity index for tropical cyclones. *Geophys. Res. Lett.*, **40**, 1878–1882, doi:10.1002/grl.50091.

Lock, A. P., A. R. Brown, M. R. Bush, G. M. Martin, and R. N. B. Smith, 2000: A new boundary layer mixing scheme. Part I: Scheme description and single-column model tests. *Mon. Wea. Rev.*, **128**, 3187–3199, doi:10.1175/1520-0493(2000)128<3187:ANBLMS>2.0.CO;2.

Merlis, T. M., M. Zhao, and I. M. Held, 2013: The sensitivity of hurricane frequency to ITCZ changes and radiatively forced warming in aquaplanet simulations. *Geophys. Res. Lett.*, **40**, 4109–4114, doi:10.1002/grl.50680.

——, W. Zhou, I. M. Held, and M. Zhao, 2016: Surface temperature dependence of tropical cyclone-permitting simulations in a spherical model with uniform thermal forcing. *Geophys. Res. Lett.*, **43**, 2859–2865, doi:10.1002/2016GL067730.

Muller, C. J., P. A. O. Gorman, and L. E. Back, 2011: Intensification of precipitation extremes with warming in a cloud-resolving model. *J. Climate*, **24**, 2784–2800, doi:10.1175/2011JCLI3876.1.

Nolan, D. S., E. D. Rappin, and K. A. Emanuel, 2007: Tropical cyclogenesis sensitivity to environmental parameters in radiative–convective equilibrium. *Quart. J. Roy. Meteor. Soc.*, **133**, 2085–2107, doi:10.1002/qj.170.

Pauluis, O., and I. M. Held, 2002a: Entropy budget of an atmosphere in radiative–convective equilibrium. Part I: Maximum work and frictional dissipation. *J. Atmos. Sci.*, **59**, 125–139, doi:10.1175/1520-0469(2002)059<0125:EBOAAI>2.0.CO;2.

——, and ——, 2002b: Entropy budget of an atmosphere in radiative–convective equilibrium. Part II: Latent heat transport and moist processes. *J. Atmos. Sci.*, **59**, 140–149, doi:10.1175/1520-0469(2002)059<0140:EBOAAI>2.0.CO;2.

Price, J. F., 1981: Upper ocean response to a hurricane. *J. Phys. Oceanogr.*, **11**, 153–175, doi:10.1175/1520-0485(1981)011<0153:UORTAH>2.0.CO;2.

Reed, K. A., and D. R. Chavas, 2015: Uniformly rotating global radiative–convective equilibrium in the Community Atmosphere Model, version 5. *J. Adv. Model. Earth Syst.*, **7**, 1938–1955, doi:10.1002/2015MS000519.

Romps, D. M., and Z. Kuang, 2010: Do undiluted convective plumes exist in the upper tropical troposphere? *J. Atmos. Sci.*, **67**, 468–484, doi:10.1175/2009JAS3184.1.

Schade, L. R., and K. A. Emanuel, 1999: The ocean's effect on the intensity of tropical cyclones: Results from a simple coupled

atmosphere–ocean model. *J. Atmos. Sci.*, **56**, 642–651, doi:10.1175/1520-0469(1999)056<0642:TOSEOT>2.0.CO;2.

Shaevitz, D. A., and Coauthors, 2014: Characteristics of tropical cyclones in high-resolution models in the present climate. *J. Adv. Model. Earth Syst.*, **6**, 1154–1172, doi:10.1002/2014MS000372.

Shen, W., and I. Ginis, 2003: Effects of surface heat flux-induced sea surface temperature changes on tropical cyclone intensity. *Geophys. Res. Lett.*, **30**, 1933, doi:10.1029/2003GL017878.

Shi, X., and C. S. Bretherton, 2014: Large-scale character of an atmosphere in rotating radiative–convective equilibrium. *J. Adv. Model. Earth Syst.*, **6**, 616–629, doi:10.1002/2014MS000342.

Tao, D., and F. Zhang, 2014: Effect of environmental shear, sea-surface temperature, and ambient moisture on the formation and predictability of tropical cyclones: An ensemble-mean perspective. *J. Adv. Model. Earth Syst.*, **6**, 384–404, doi:10.1002/2014MS000314.

Vincent, E. M., K. A. Emanuel, M. Lengaigne, J. Vialard, and G. Madec, 2014: Influence of upper ocean stratification interannual variability on tropical cyclones. *J. Adv. Model. Earth Syst.*, **6**, 680–699, doi:10.1002/2014MS000327.

Walsh, K. J. E., and Coauthors, 2015: Hurricanes and climate: The U.S. CLIVAR Working Group on Hurricanes. *Bull. Amer. Meteor. Soc.*, **96**, 997–1017, doi:10.1175/BAMS-D-13-00242.1.

Wing, A. A., S. J. Camargo, and A. H. Sobel, 2016: Role of radiative–convective feedbacks in spontaneous tropical cyclogenesis in idealized numerical simulations. *J. Atmos. Sci.*, **73**, 2633–2642, doi:10.1175/JAS-D-15-0380.1.

Zhao, M., I. M. Held, S. J. Lin, and G. A. Vecchi, 2009: Simulations of global hurricane climatology, interannual variability, and response to global warming using a 50-km resolution GCM. *J. Climate*, **22**, 6653–6678, doi:10.1175/2009JCLI3049.1.

——, ——, and S.-J. Lin, 2012: Some counterintuitive dependencies of tropical cyclone frequency on parameters in a GCM. *J. Atmos. Sci.*, **69**, 2272–2283, doi:10.1175/JAS-D-11-0238.1.

Zhou, W., 2015: The impact of vertical shear on the sensitivity of tropical cyclogenesis to environmental rotation and thermodynamic state. *J. Adv. Model. Earth Syst.*, **7**, 1872–1884, doi:10.1002/2015MS000543.

——, I. M. Held, and S. T. Garner, 2014: Parameter study of tropical cyclones in rotating radiative–convective equilibrium with column physics and resolution of a 25-km GCM. *J. Atmos. Sci.*, **71**, 1058–1069, doi:10.1175/JAS-D-13-0190.1.

Zhu, T., and D.-L. Zhang, 2006: The impact of the storm-induced SST cooling on hurricane intensity. *Adv. Atmos. Sci.*, **23**, 14–22, doi:10.1007/s00376-006-0002-9.